Journal of Magnetism and Magnetic Materials 342 (2013) 139–143

Contents lists available at SciVerse ScienceDirect

Journal of Magnetism and Magnetic Materials

journal homepage: www.elsevier.com/locate/jmmm

Current-induced spin polarization on a Pt surface: A new approach using spin-polarized positron annihilation spectroscopy

A. Kawasuso [a,*], Y. Fukaya [a], M. Maekawa [a], H. Zhang [a], T. Seki [b], T. Yoshino [b], E. Saitoh [b], K. Takanashi [b]

[a] Advanced Science Research Center, Japan Atomic Energy Agency, 1233 Watanuki, Takasaki, Gunma 370-1292, Japan
[b] Institute for Materials Research, Tohoku University, 2-1-1 Katahira, Aoba-ku, Sendai 980-8577, Japan

ARTICLE INFO

Article history:
Received 16 December 2012
Available online 24 April 2013

Keywords:
Positron annihilation
Positronium
Surface magnetism
Surface spin accumulation

ABSTRACT

Transversely spin-polarized positrons were injected near Pt and Au surfaces under an applied electric current. The three-photon annihilation of spin-triplet positronium, which was emitted from the surfaces into vacuum, was observed. When the positron spin polarization was perpendicular to the current direction, the maximum asymmetry of the three-photon annihilation intensity was observed upon current reversal for the Pt surfaces, whereas it was significantly reduced for the Au surface. The experimental results suggest that electrons near the Pt surfaces were in-plane and transversely spin-polarized with respect to the direction of the electric current. The maximum electron spin polarization was estimated to be more than 0.01 (1%).

1. Introduction

Current-induced spin polarization (CISP) on non-magnetic material surfaces has attracted much attention due to the rapid development of spintronics devices and their underlying physics. Spin current arises from the spin–orbit (SO) interaction between the conduction electrons and nuclei, which then causes CISP [1–9]. The Rashba SO interaction, which originates from space-reversal symmetry-breaking at a surface, gives rise to CISP near surfaces and interfaces [7–9]. The surface boundary conditions, as well as surface structure and electronic state, affect CISP.

Reducing the coordination number of the surface atoms results in band narrowing and strong electron localization. Surface lattice distortion also modulates the electronic state of the surface; therefore, the magnetic properties of surface may be different from those of the bulk. Some theoretical studies have predicted the appearance of a large magnetic moment on Pt surfaces, even though the bulk is paramagnetic [10,11]. Thus, it is particularly interesting to use newly developed surface-sensitive tools to investigate CISP on Pt [12–16] and Au [17] surfaces, where large spin currents are observed.

Spin-polarized positron annihilation spectroscopy is a possible probe for observing electron spin polarization on metal surfaces. Spin-polarized electrons can be detected through either free annihilation between positrons and electrons or self-annihilation of positronium, which is a bound state of a positron and an electron. The former has recently been used to study ferromagnetic band structures [18,19]. The latter positronium method should be well suited to the detection of spin-polarized conduction electrons at the outermost surface layer; when positroniums are emitted into vacuum, positrons pick up surface electrons near the Fermi level. A pioneering study of the surface magnetism of Ni [20] demonstrated that this method has an extremely high surface selectivity, which can be applied to bare surfaces without device fabrication. The detection limit of spin polarization is low (10^{-3} (0.1%)) for normal positron spin polarization (≈30%) using conventional sources. These are major advantages for studying surface spin phenomena.

In this paper, we describe CISP on Pt and Au surfaces, as investigated by spin-polarized positron annihilation spectroscopy based on the positronium method. For Pt surfaces, the spin polarization of surface electrons near the Fermi level was a few percent. We discuss the possible reasons for this large CISP on the Pt surfaces in relation to the Rashba effect and the ferromagnetism associated with the outermost surface state.

2. Method and materials

2.1. Method

We first summarize the principles underpinning our method. A portion of the positrons injected into a sample diffuse back to the surface, pick up surface electrons near the Fermi level, and

* Corresponding author. Tel.: +81 273469331; fax: +81 273469432.
E-mail address: kawasuso.atsuo@jaea.go.jp (A. Kawasuso).

0304-8853/$ - see front matter © 2013 Published by Elsevier B.V.
http://dx.doi.org/10.1016/j.jmmm.2013.04.006

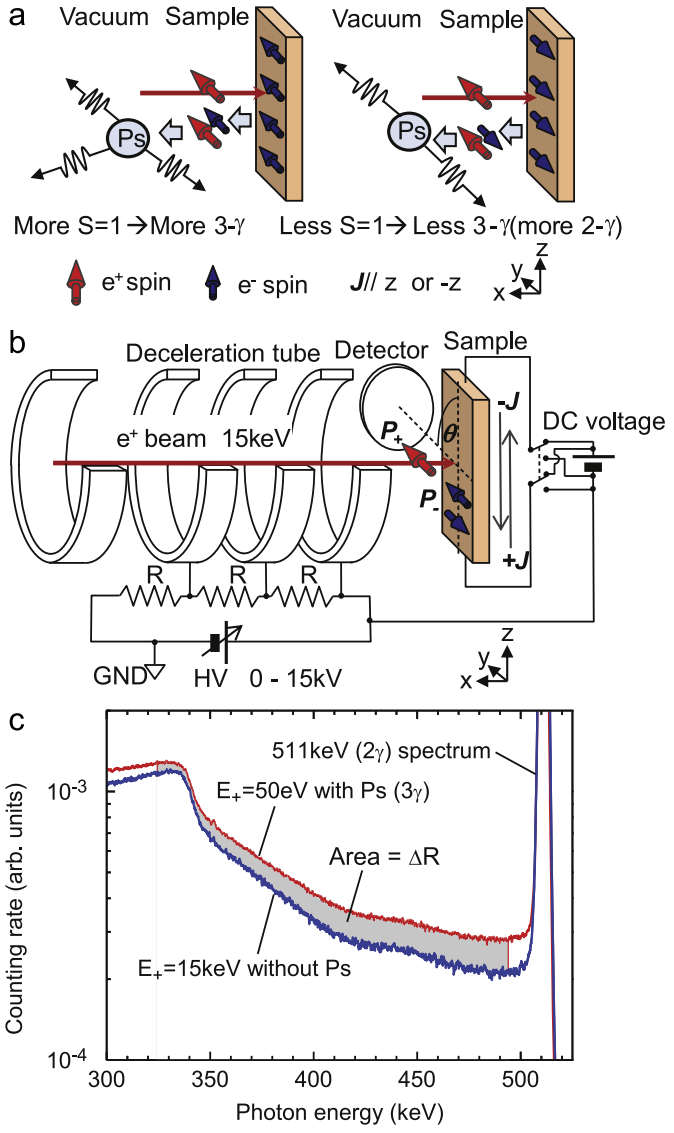

Fig. 1. (a) Principles of the present spin-polarized positron annihilation spectroscopy. Transversely polarized positrons are injected into the sample under an electric current applied along the z-axis. The implanted positrons diffuse back to the surface and form positronium (Ps) with the surface conduction electrons. The positron polarization direction ($\mathbf{P}_+$) is fixed and the electron polarization direction ($\mathbf{P}_-$) is changed by current reversal ($+j \leftrightarrow -j$). The fractions of each spin state of positronium are also changed by current reversal. The relationship between the electron polarization and the current direction is not known *a priori*. (b) Experimental setup. Transversely polarized positrons with energy of 15 keV are injected into the sample under electric current. Positron energy is adjusted to below 15 keV by a deceleration tube. An annihilation photon detector is set perpendicular to the beam axis. The angle between the positron polarization and current direction, θ, is changed by rotating the sample holder. (c) Energy spectra of annihilation photons obtained for the Pt/Fe/MgO sample at $E_+ = 15$ keV and 50 eV. The intensity is normalized to the 511 keV area intensity. The gray area denotes ΔR. Similar spectra were obtained for the other samples.

escape into the vacuum as positronium (Fig. 1(a)). The allowed spin states of positronium are the spin-singlet state ($S=0$ and $m=0$; $|00\rangle$) and spin-triplet state ($S=1$ and $m=0, \pm 1$; $|10\rangle$, $|11\rangle$ or $|1{-}1\rangle$), where S and m are the total spin and the magnetic quantum number, respectively. These spin wave functions are $|00\rangle = |\Uparrow\downarrow\rangle - |\Downarrow\uparrow\rangle$, $|10\rangle = |\Uparrow\downarrow\rangle + |\Downarrow\uparrow\rangle$, $|11\rangle = |\Uparrow\uparrow\rangle$ and $|1{-}1\rangle = |\Downarrow\downarrow\rangle$, respectively, where the thick arrows denote positrons and thin arrows denote electrons. Spin-singlet positronium decays into two photons, and spin-triplet positronium decays into three photons. It is assumed that the positrons are always transversely polarized (y direction) with a net polarization of P_+. Fractions of each positronium spin state are given by

$$F_{|00\rangle} = (1 - P_+P_- \cos\varphi)/4, \tag{1}$$

$$F_{|10\rangle} = (1 - P_+P_- \cos\varphi)/4, \tag{2}$$

$$F_{|11\rangle} = (1 + P_+ + P_- \cos\varphi + P_+P_- \cos\varphi)/4, \tag{3}$$

$$F_{|1-1\rangle} = (1 - P_+ - P_- \cos\varphi + P_+P_- \cos\varphi)/4, \tag{4}$$

where P_- is the electron polarization and φ is the angle between the positron and the electron polarization directions. The two-photon annihilation fraction is given by $F_{Ps}^{2\gamma} = F_{|00\rangle}$. The total three-photon annihilation fraction is given by

$$F_{Ps}^{3\gamma} = \epsilon(1)(F_{|11\rangle} + F_{|1-1\rangle}) + \epsilon(0)F_{|10\rangle}, \tag{5}$$

where $\epsilon(1)$ and $\epsilon(0)$ are the detection efficiencies of annihilation photons from the $m = \pm 1$ and $m=0$ states, respectively. This efficiency also depends on the angle between the direction of the detector and the positron polarization [21]. When the positron and electron polarization directions are the same (Fig. 1(a), left), the $|11\rangle$ state is preferentially formed and the fractions of the other states are lower, resulting in the increase in $F_{Ps}^{3\gamma}$ and the decrease in $F_{Ps}^{2\gamma}$. Conversely, when the positron and electron polarization directions are reversed (Fig. 1(a), right), the fractions of the $|11\rangle$ and $|1{-}1\rangle$ states are lower compared with the $|10\rangle$ and $|00\rangle$ states. Hence, $F_{Ps}^{3\gamma}$ decreases and $F_{Ps}^{2\gamma}$ increases.

In the annihilation photon energy spectrum, the two-photon annihilation produces a peak at 511 keV ($= m_0c^2$) with a finite width, whereas the intensity of the three-photon annihilation continuously increases from 0 to 511 keV (see Fig. 1(c)). The two-photon annihilation spectrum shows the free annihilation of positrons and electrons inside the sample and the self-annihilation of positronium emitted into the vacuum. Because the probability of the three-photon annihilation between positrons and electrons inside a sample is negligible (1/371), the observed three-photon annihilation comes only from positroniums emitted into the vacuum. The positronium three-photon annihilation is traditionally characterized by a quantity R [22],

$$R = (T-U)/U = \frac{(1-F_{Ps}^{3\gamma})R_0 + F_{Ps}^{3\gamma}R_1U_1/U_0}{1-F_{Ps}^{3\gamma} + F_{Ps}^{3\gamma}U_1/U_0}, \tag{6}$$

where T is the area under the entire intensity curve, U is the area under the two-photon annihilation spectrum, and the subscripts 0 and 1 denote 0% and 100% positronium emission, respectively. Although R is a complicated function of $F_{Ps}^{3\gamma}$, for its small value as in the present case, $\Delta R = R - R_0$ is approximately proportional to $F_{Ps}^{3\gamma}$. Thus, Eqs. (2)–(6) can be used to express the asymmetry of ΔR upon spin flip ($+P_- \leftrightarrow -P_-$) as

$$A = \frac{\Delta R(+P_-) - \Delta R(-P_-)}{\Delta R(+P_-) + \Delta R(-P_-)} = \frac{2\epsilon(1) - \epsilon(0)}{2\epsilon(1) + \epsilon(0)} P_+P_- \cos\varphi. \tag{7}$$

The direction of the electron spin polarization can be changed by the current reversal ($+j \leftrightarrow -j$). Accordingly, CISP can be detected by the change of ΔR upon current reversal. The two-photon annihilation of positronium mirrors the change in ΔR, providing it is not masked by the two-photon annihilation of positrons and electrons inside the sample.

Fig. 1(b) shows a schematic of the experimental setup. The samples are mounted on a plate holder, and an electric current is applied through two electrodes on the edges of the samples in the direction shown in the figure. The finite spin polarization of the conduction electrons perpendicular to the current direction may appear near the surface if CISP occurs. The relationship between the current and the electron spin-polarization directions is not known *a priori*. In the present experiment, a positron beam with an energy of $E_+ = 15$ keV is electrostatically generated by using a

^{22}Na source (370 MBq) and a tungsten mesh moderator. The longitudinal spin polarization of the positron beam is determined as $P_+ = 0.3$ [23]. The beam is bent 90° using a plate deflector. This transversely (y direction) polarized positron beam is directed onto the sample at normal incidence. The beam energy is adjusted to below 15 keV by using a deceleration tube under high voltage. The angle θ between the current and positron polarization directions is changed by rotating the sample around the beam axis. The energy spectrum of the annihilation photons is measured by a Ge detector set perpendicular to the beam axis. The efficiency function $(2\epsilon(1)-\epsilon(0))/(2\epsilon(1)+\epsilon(0))$ in Eq. (7) is approximately 0.6.

2.2. Materials

The samples used in this study were Pt(001) and Au(001) single-crystal films (10 × 20 mm, 50 nm thick) grown epitaxially on Fe(001) seed layers (1 nm thick) on MgO(001) substrates by magnetron sputtering in an ultrahigh vacuum chamber (2×10^{-7} Pa) at room temperature, and are referred to as Pt/Fe/MgO and Au/Fe/MgO, respectively. A polycrystalline Pt film without an Fe layer was also grown directly on a MgO(001) substrate, and is referred to as Pt/MgO.

3. Results and discussion

Fig. 1(c) shows the typical annihilation photon energy spectra obtained for the Pt/Fe/MgO sample at $E_+ = 50$ eV and 15 keV. Similar spectra were obtained for the other samples. The total intensity was normalized to the area intensities of the two-photon annihilation spectra. At $E_+ = 15$ keV, the positronium fraction was neglected because the positrons were injected deep into the sample. The non-zero intensity below 511 keV was mainly caused by the Compton scattering of 511 keV photons. When the incident positron energy is low enough, most positrons diffuse back to the surface. Four processes occur at the surface: (i) positron re-emission, (ii) positron surface trapping, (iii) positronium emission, and (iv) positronium surface trapping. The increased intensity below 511 keV in the energy spectrum for $E_+ = 50$ eV indicates the positronium emission and the three-photon annihilation. The difference in the low-energy tail intensities around 480 keV for the 100% and 0% positronium emissions has been reported to be 0.033 for an Al(110) surface [24]. The difference in intensities for $E_+ = 50$ eV and 15 keV was approximately 0.003 for our samples; therefore the maximum positronium emission was 10% (0.003/0.033~0.1). To evaluate the positronium emission more precisely, a reference spectrum with a known positronium emission would be required. The positronium emission observed here is consistent with the negative work functions for Pt and Au. The sample temperatures were measured as approximately 250 °C due to Joule heating. This was not high enough to generate thermal vacancies which alter the detection of CISP. The sample heating enhanced the positronium emission, because of the effect of surface cleaning and the thermal activation of positronium [22].

Fig. 2 shows the ΔR and 511 keV peak intensity normalized to its area intensity for the Pt/Fe/MgO sample in successive measurements upon current reversal at $E_+ = 50$ eV and $\theta = 90°$. The value of ΔR oscillated, which shows that surface electrons were in-plane spin-polarized and the polarization direction was reversed by switching the current direction. The higher ΔR corresponds to $\Uparrow + \uparrow$ (left), and the lower corresponds to $\Uparrow + \downarrow$ (right) in Fig. 1(a). The oscillation of ΔR decreased as E_+ increased above 200 eV, which suggests that it was caused by the positronium emission from the surface. The oscillation of the 511 keV peak intensity appeared to be very small. The maximum positronium emission was 10%. In addition, $F_{Ps}^{2\gamma}$ was only ≈1/4 of the total positronium fraction, when

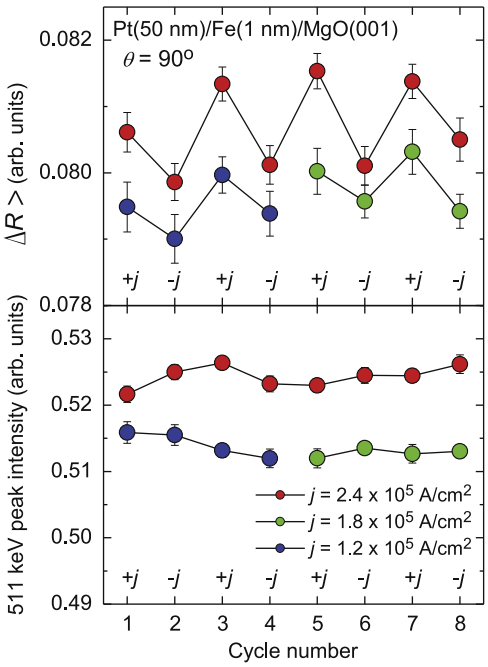

Fig. 2. ΔR and 511 keV peak intensity normalized to its area intensity as a function of the current reversal cycle number for the Pt/Fe/MgO sample with current densities of $j = 1.2\times10^5$ A/cm^2, 1.8×10^5 A/cm^2 and 2.4×10^5 A/cm^2 at $E_+ = 50$ eV and at $\theta = 90°$.

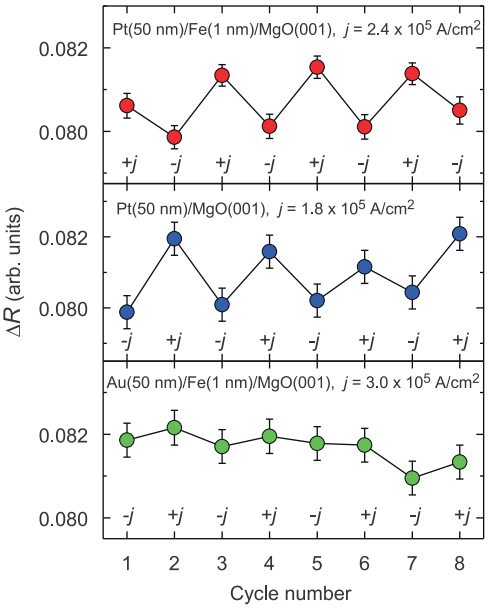

Fig. 3. ΔR as a function of the current reversal cycle number for the Pt/Fe/MgO, Pt/MgO, and Au/Fe/MgO samples with current densities of $j = 2.4\times10^5$ A/cm^2, 1.8×10^5 A/cm^2 and 3.0×10^5 A/cm^2, respectively, at $E_+ = 50$ eV and $\theta = 90°$.

P_- was not sufficiently high. The change in the 511 keV peak intensity caused by positronium was overcompensated by abundant free positron annihilation.

Fig. 3 shows the successive current reversal of ΔR obtained for the Pt/MgO, Au/Fe/MgO, and Pt/Fe/MgO samples. For the Pt/MgO sample, the oscillation of ΔR was similar to the Pt/Fe/MgO sample. This suggests that the Fe layer was not essential for the appearance of ΔR oscillation. The oscillation of ΔR for the Au/Fe/MgO sample

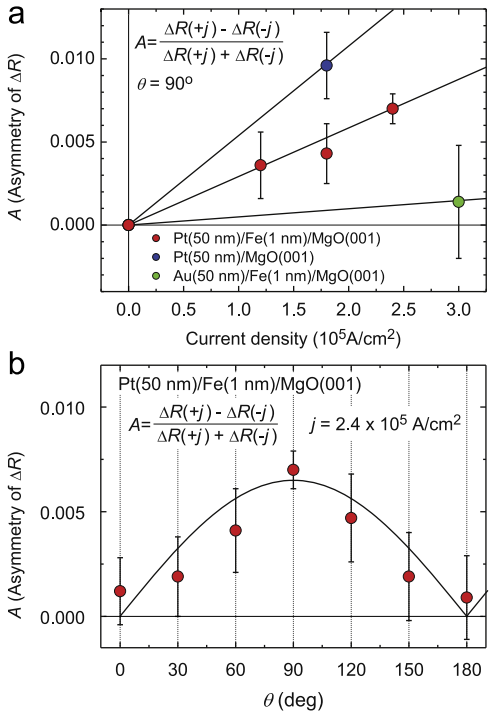

Fig. 4. (a) Asymmetry (A) of ΔR as a function of the current density for the Pt/Fe/MgO, Pt/MgO, and Au/Fe/MgO samples at $E_+ = 50$ eV and $\theta = 90^\circ$. (b) Asymmetry (A) of ΔR as a function of angle θ between the positron polarization and current direction for the Pt/Fe/MgO sample at $j = 2.4 \times 10^5$ A/cm^2 and $E_+ = 50$ eV. The solid line is the $\sin\theta$ curve.

had a significantly smaller amplitude compared with the Pt samples. Fig. 4(a) shows the asymmetry of ΔR as a function of current density for all the samples. Fig. 4(b) shows that the asymmetry for the Pt/Fe/MgO sample increased from $\theta = 0^\circ$, reached a maximum at $\theta = 90^\circ$, and then decreased until $\theta = 180^\circ$. Because the maximum asymmetry occurred at $\theta = 90^\circ$, $\varphi = \theta - 90^\circ$. The asymmetry of ΔR was proportional to the $\sin\theta$ curve.

These results suggest that electrons near the Pt surfaces are in-plane and transversely spin-polarized with respect to the electric current direction. The current directions $+j$ and $-j$ corresponded to the spin directions $\Uparrow + \uparrow$ (left) and $\Uparrow + \downarrow$ (right), respectively, in Fig. 1(a). The magnetic field generated by the electric current was calculated as less than 1 mT using the Biot-Savart principle, which was too small to affect the positron beam and the positronium annihilation characteristics. The spin polarization of the surface electrons for the Pt/Fe/MgO sample was estimated to be $P_- \approx 0.04$ from Eq. (7) using the positron polarization $P_+ = 0.3$ and the asymmetry of ΔR in Fig. 4(a) ($j = 2.4 \times 10^5$ A/cm^2) and $P_- \approx 0.06$ for the Pt/MgO sample ($j = 1.8 \times 10^5$ A/cm^2).

The relationship between the accumulated spin and the current directions was the same as that observed in a previously reported electrotransport experiment [25] and that predicted from theory [26]. This was explained by the negative *LS* coupling of the *sd* band in Pt because of the occupation of the *d*-orbital with 9 electrons. The sign change of the SO coupling for transition metals with different numbers of *d* electrons was also observed in these experimental and theoretical studies. The spin Hall conductivity of Au is predicted to be much smaller than that of Pt, which reflects the closed (Au)- and open (Pt)-*d*-shell structures [26]. Therefore, the CISP observed here could have originated from the spin Hall effect.

However, the magnitude of the CISP was not explicitly interpreted using the framework of the spin Hall effect. According to spin diffusion theory [27], the electron polarization on a surface is given as the shift of the chemical potential; $\Delta\mu \approx 2\alpha_{SH}\lambda_S j/\sigma$, where α_{SH}, λ_S, and σ are the spin Hall angle, the spin diffusion length (≈10 nm), and the electrical conductivity ($\approx 2.5 \times 10^4\ \Omega^{-1}\ \mathrm{cm}^{-1}$ for Pt), respectively. The spin Hall angle of Pt is $0.05 < \alpha_{SH} < 0.16$ [16]. Consequently, for the present current densities the value of P_- predicted by spin diffusion theory is of the order of 10^{-5}, which is three orders of magnitude smaller than the experimental value of P_-. There are no established theories to explain the large CISP for the Pt surfaces. One possible explanation may be the surface Rashba effect, which induces a much stronger spin accumulation than that expected from spin diffusion theory. In relation to the magnetism, the Stoner parameter of bulk Pt is relatively high [28] and it may readily be enhanced at the first surface layer by the reduction of the coordination number and the lattice distortion [11,10]. In contrast, the Stoner parameter of bulk Au is small. Therefore, the current-induced spin accumulation on the Pt surface may be enhanced further by inducing ferromagnetic order.

4. Conclusions

In conclusion, spin-polarized positron annihilation spectroscopy was used to observe the CISP on Pt and Au surfaces. A large CISP was observed for the Pt surfaces, whereas it was suppressed for the Au surface. Although this was related to the SO interaction of Pt and Au, further experimental and theoretical studies are required to fully explain the magnitude of CISP. Our study demonstrates that spin-polarized positron annihilation spectroscopy provides a unique tool for investigating spin polarization on metal surfaces.

Acknowledgments

We thank S. Maekawa and J. Ieda of the Japan Atomic Energy Agency for their valuable comments. This work was supported by the JSPS KAKENHI Grant no. 24310072.

References

[1] M.I. Dyakonov, V.I. Perel, Physics Letters 35A (1971) 459.
[2] J.E. Hirsch, Physical Review Letters 83 (1999) 1834.
[3] S. Zhang, Physical Review Letters 85 (2000) 393.
[4] S.O. Valenzuela, M. Tinkham, Nature 422 (2006) 176.
[5] Y.K. Kato, R.C. Myers, A.C. Gossard, D.D. Awschalom, Science 306 (2004) 1910.
[6] J. Wunderlich, J. Sinova, T. Jungwirth, Physical Review Letters 047204 (2005) 94.
[7] J. Sinova, D. Culcer, Q. Niu, N.A. Sinitsyn, T. Jungwirth, A.H. MacDonald, Physical Review Letters 26 (2004) 126603.
[8] Y.K. Kato, R.C. Myers, A.C. Gossard, D.D. Awschalom, Physical Review Letters 93 (2004) 176601.
[9] I.M. Miron, G. Gaudin, S. Auffret, B. Rodmacq, A. Schuhl, S. Pizzini, J. Vogel, P. Gambardella, Nature Materials 9 (2010) 230.
[10] L.H. Yang, J. Park, B.D. Yu, Journal of the Korean Physical Society 56 (2010) 791.
[11] S. Blügel, Physical Review B 51 (1995) 2025.
[12] T. Kimura, Y. Otani, T. Sato, S. Takahasi, S. Maekawa, Physical Review Letters 98 (2007) 156601.
[13] E. Saitoh, M. Ueda, H. Miyajima, G. Tatara, Applied Physics Letters 88 (2006) 182509.
[14] K. Ando, S. Takahashi, K. Harii, K. Sasage, J. Ieda, S. Maekawa, E. Saitoh, Physical Review Letters 101 (2008) 036601.
[15] O. Mosendz, J.E. Pearson, F.Y. Fradin, G.E. Bauer, S.D. Bader, A. Hoffmann, Physical Review Letters 104 (2010) 046601.
[16] L. Liu, T. Moriyama, D.C. Ralph, R.A. Buhrman, Physical Review Letters 106 (2011) 036601.
[17] T. Seki, Y. Hasegawa, S. Mitani, S. Takahashi, H. Imamura, S. Maekawa, J. Nitta, K. Takanashi, Nature Materials 7 (2008) 125.
[18] A. Kawasuso, M. Maekawa, Y. Fukaya, A. Yabuuchi, I. Mochizuki, Physical Review B 83 (2011) 100406(R).
[19] A. Kawasuso, M. Maekawa, Y. Fukaya, A. Yabuuchi, I. Mochizuki, Physical Review B 85 (2012) 024417.
[20] D.W. Gidley, A.R. Köymen, T.W. Capehart, Physical Review Letters 49 (1982) 1779.
[21] R.M. Drisko, Physical Review 102 (1956) 1542.
[22] K.G. Lynn, D.O. Welch, Physical Review B 22 (1980) 99.

[23] A. Kawasuso, M. Maekawa, Applied Surface Science 255 (2008) 108.
[24] J. Lahtinen, A. Vehanen, H. Huomo, J. Mäkinen, P. Huttunen, K. Rytsölä, M. Bentzon, P. Hautojärvi, Nuclear Instruments and Methods in Physics Research B 17 (1986) 73.
[25] M. Morota, Y. Niimi, K. Ohnishi, D.H. Wei, T. Tanaka, H. Kotani, T. Kimura, Y. Otani, Physical Review B 83 (2011) 174405.
[26] T. Tanaka, H. Kotani, M. Naito, T. Naito, D.S. Hirashima, K. Yamada, J. Inoue, Physical Review B 77 (2008) 165117.
[27] S. Takahashi, H. Imamura, S. Maekawa, Spin injection and spin transport in hybrid nanostructures, in: S. Maekawa (Ed.), Concepts in Spin Electronics, Oxford University Press, Oxford, 2006, p. 343.
[28] M.M. Sigalas, D.A. Papaconstantopoulos, Physical Review B 50 (1994) 7255.